

A Fully Polarimetric Multiple Scattering Model for Crops

M. Bracaglia,* P. Ferrazzoli,* and L. Guerriero*

This article describes an electromagnetic model which simulates the microwave polarimetric backscatter of agricultural fields. The model is based on radiative transfer theory and solves the relevant equation by means of a numerical algorithm, namely matrix doubling, which includes multiple scattering effects. The backscatter coefficient may be simulated for any pair of incidence and scattering elliptical polarizations; also, the phase difference between VV and HH channels is computed. Model simulations are compared with experimental results obtained at L band (1.2 GHz) by the NASA-JPL AIRSAR, in the framework of the MAC Europe '91 campaign, over sunflower fields belonging to an Italian site named Montespertoli. A satisfactory agreement is observed between predicted and measured polarimetric quantities of vegetated fields, while for bare soils (particularly at VV polarization) backscatter coefficients are overestimated, due to inaccuracies of surface models available at present.

INTRODUCTION

Several experimental and theoretical studies have been carried out in the last years to investigate the sensitivity of radar systems to the properties of agricultural fields. Ground-based scatterometer data have been obtained in the USA since the 1970s, and results are now available in systematic form (Ulaby and Dobson, 1989). Airborne campaigns took place in Europe in the summers of 1986, 1987, and 1988 (Bouman and Hoekman, 1993; Ferrazzoli et al., 1992; Prevot et al., 1993). More recent experiments, carried out in 1989 and 1991, used the

fully polarimetric AIRSAR (Churchill and Attema, 1992; Wickland et al., 1993).

Interpretation of experimental data is a complex task, since the radar response is affected by many parameters, like soil moisture, soil roughness, crop biomass, plant moisture content, and plant geometry (i.e., shape, dimensions, orientation, and relative location of vegetation elements). Moreover, the sensitivity to the different medium parameters is much affected by the sensor configuration (i.e., frequency, polarization, and incidence angle), and a wide variability of geometrical and physical properties characterize the various crops. To understand the interactions between microwaves and vegetation, the utility of electromagnetic models has been extensively recognized. Models give a physical basis to experimental correlations between radar response and medium parameters, allow identification of the different scattering sources within the canopy, and make it possible to carry out parametric investigations.

Originally, a simple model was proposed by Attema and Ulaby (1978) that describes vegetation as an ensemble of identical scatterers, whose attenuation and scattering properties are obtained, for each crop, by fitting experimental data. This approach, in spite of its simplicity, allowed interpretation of some experimental results obtained by copolar scatterometers. However, to get an insight into vegetation scattering and to interpret data obtained by polarimetric systems, which have become available in the recent years, more advanced approaches have been proposed. A vertical cylindrical structure has been used by Ulaby et al. (1987) to explain the VV-HH phase differences measured over corn fields. More recently, canopies consisting of discs and cylinders have been introduced. In particular, Chauhan et al. (1994) modeled corn at HH and VV polarization using the distorted Born approximation, Tourè et al. (1994) used radiative transfer theory to model wheat and canola at HH and VV polarization, and a two-scale branching scattering model was introduced by Yueh et al. (1992)

* Dipartimento di Ingegneria Elettronica, Università Tor Vergata, Rome

Address correspondence to P. Ferrazzoli, Università Tor Vergata, Dipartimento di Ingegneria Elettronica, Via della Ricerca Scientifica, 00133 Roma, Italy.

Received 23 February 1995; revised 28 June 1995.

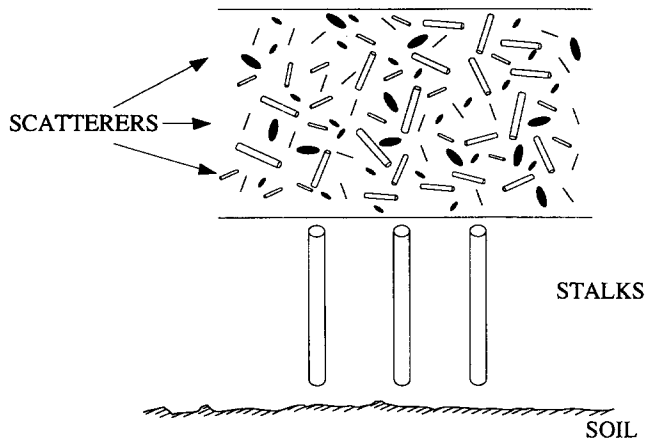


Figure 1. Sketch used to model crops.

for soybeans at HH, VV, and HV polarizations. Fairly good agreements have been observed with experimental results in all the three cases.

Also the model implemented by us describes vegetation as an ensemble of discs and cylinders (Ferrazzoli et al., 1991; Ferrazzoli and Guerriero, 1994; 1995). Radiative transfer theory is used: The equation is solved by a numerical algorithm, namely matrix doubling, which includes multiple scattering effects. The model, in the version described in this article, is fully polarimetric: The backscatter coefficient for any pair of incidence and scattering polarizations is computed, as well as the VV–HH phase difference. The numerical procedure is described in the next section, while the third section shows a comparison between polarimetric features measured over sunflower fields at different stages of growth and those predicted by the model. The comparison is done at L band (1.2 GHz) and at linear horizontal, linear vertical, linear 45°, and circular incidence polarizations. Both the copolar and the crosspolar responses are considered. Finally, the predicted and measured (VV–HH) phase differences are compared.

THE MODEL

Geometry Selection

Similarly to most of the microwave vegetation models available now, an infinite half-space with rough interface is used to describe the soil, while an ensemble of discrete scatterers is used to describe the canopy. Simple geometries, for which electromagnetic approximations are available, are assumed for scatterers: Discs describe leaves, while cylinders describe stems. Once the scatterer geometries are selected, the problem of scatterer location within the canopy has to be considered. In this article the simple configuration indicated in Figure 1 is selected, including a uniform top layer of discs (leaves) and cylinders (stems), an intermediate ensemble of large

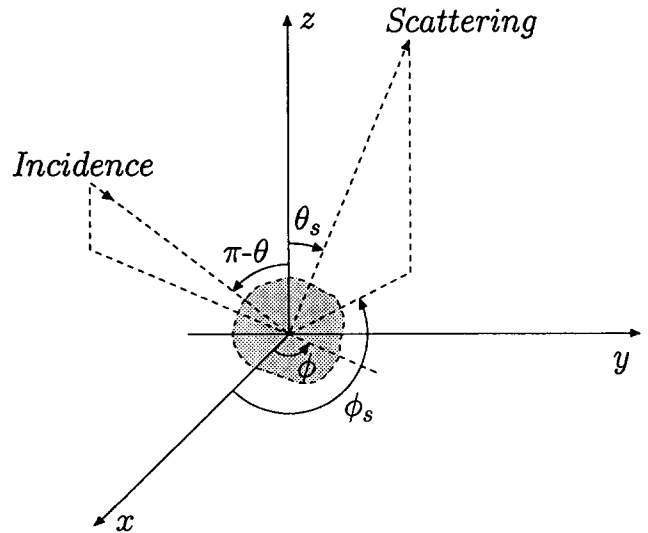


Figure 2. Scatterer reference system: θ = off-normal angle of incidence direction, φ = azimuth angle of incidence direction, θ_s = off-normal angle of scattering direction, and φ_s = azimuth angle of scattering direction.

vertical cylinders (main stalks), and an infinite dielectric half-space (soil). This configuration, which will be used in the next section to test the model with experimental results obtained over sunflower fields, is realistic for some crops, like sunflower and corn; for other crops, other geometries, which include cylindrical vertical elements on top (like wheat ears), are more suitable (Ferrazzoli et al., 1995a).

Single Scatterer

The single scatterer is characterized by the complex “scattering amplitude” (Ishimaru, 1978) $f_{pq}(\theta, \varphi; \theta_s, \varphi_s)$ which is a function of incidence direction (θ, φ), scattering direction (θ_s, φ_s), incidence polarization ($q = V, H$) and scattering polarization ($p = V, H$) (Fig. 2). $f_{pq}(\theta, \varphi; \theta_s, \varphi_s)$ depends on shape, dimensions, orientation, and permittivity of the scatterer. The following types of scatterers are considered by us:

- Discs under the Rayleigh–Gans approximation model leaves when $\sqrt{\epsilon_r} k \delta_d \ll 1$, where ϵ_r is the permittivity, k is the free-space wavenumber, and δ_d is the disc thickness. The scattering amplitude is given by Schiffer and Thielheim (1979) and Eom and Fung (1984).
- Discs under the physical optics approximation model leaves when $ka_d \gg 1$, where a_d is the disc radius. The scattering amplitude is given by Le Vine et al. (1983).
- Needles under the Rayleigh–Gans approximation model stems when $\sqrt{\epsilon_r} k a_n \ll 1$, where a_n is the needle radius. The scattering amplitude is taken from Eom and Fung (1986).

- Cylinders under the “infinite length” approximation model stems when $kl_c \gg 1$, where l_c is the cylinder semi-length. The scattering amplitude is given by Karam and Fung (1988).

In all the four cases the scatterer permittivity is computed through the semiempirical formula given by El-Rayes and Ulaby (1987), which needs the moisture content and the dry matter density as inputs. Scatterer orientation is expressed by the Eulerian angles α , β , and γ (Eom and Fung, 1984). For a given scatterer, the complex quantities: $f_{vv}(\theta, \varphi; \theta_s, \varphi_s)$, $f_{vh}(\theta, \varphi; \theta_s, \varphi_s)$, $f_{hv}(\theta, \varphi; \theta_s, \varphi_s)$, and $f_{hh}(\theta, \varphi; \theta_s, \varphi_s)$ are computed. The 4×4 average modified Mueller matrix (or “phase matrix”), given by Ishimaru (1978), Tsang et al. (1985), and Kuga et al. (1990) is then obtained:

$$[\sigma] = 4\pi \times \begin{bmatrix} \langle |f_{vv}|^2 \rangle & \langle |f_{vh}|^2 \rangle & \langle \text{Re}(f_{vh}^* f_{vv}) \rangle & \langle -\text{Im}(f_{vh}^* f_{vv}) \rangle \\ \langle |f_{vh}|^2 \rangle & \langle |f_{hh}|^2 \rangle & \langle \text{Re}(f_{hh}^* f_{vh}) \rangle & \langle -\text{Im}(f_{hh}^* f_{vh}) \rangle \\ 2 \langle \text{Re}(f_{vv} f_{hh}^*) \rangle & 2 \langle \text{Re}(f_{vh} f_{hh}^*) \rangle & \langle \text{Re}(F^+) \rangle & \langle -\text{Im}(F^+) \rangle \\ 2 \langle \text{Im}(f_{vv} f_{hh}^*) \rangle & 2 \langle \text{Im}(f_{vh} f_{hh}^*) \rangle & \langle \text{Im}(F^+) \rangle & \langle \text{Re}(F^+) \rangle \end{bmatrix}, \quad (1)$$

where

$$F^+ = (f_{vv} f_{hh}^* + f_{vh} f_{hv}^*),$$

$$F^- = (f_{vv} f_{hh}^* - f_{vh} f_{hv}^*).$$

A factor 4π is included, which makes elements of $[\sigma]$ “polarized bistatic scattering cross-sections” (m^2), to be used in the next subsection to compute scatterer layer matrices. Averaging is carried out among the different scatterer types and, for each scatterer type, over α , β , and γ . In this article, we assume azimuthal symmetry (i.e., α uniformly contributed between 0 and 2π), which makes the 16 matrix elements depend on the $\varphi_s - \varphi$ difference, instead of φ and φ_s separately; of course, they are also dependent on θ and θ_s .

The phase matrix $[\sigma]$ describes the scattering properties of the object. To characterize the propagation effects, in amplitude and phase, a 4×4 extinction matrix $[\sigma_e]$ is given by Tsang et al. (1985) and Kuga et al. (1990), defined as

$$[\sigma_e] = \begin{bmatrix} \sigma_{ev} & 0 & 0 & 0 \\ 0 & \sigma_{eh} & 0 & 0 \\ 0 & 0 & 0.5(\sigma_{ev} + \sigma_{eh}) & \beta_v - \beta_h \\ 0 & 0 & -\beta_v + \beta_h & 0.5(\sigma_{ev} + \sigma_{eh}) \end{bmatrix}, \quad (2)$$

where

$$\sigma_{eq} = \frac{4\pi}{k} \text{Im} \langle f_{qq}^r \rangle,$$

$$\beta_q = \frac{2\pi}{k} \text{Re} \langle f_{qq}^r \rangle.$$

$\langle f_{qq}^r \rangle$ is the average scattering amplitude computed in the forward direction, that is, at $\theta_s = \theta$ and $\varphi_s - \varphi = 0$. The elements of $[\sigma_e]$ are functions of θ .

Scatterer Layer

The vegetation layer, filled with scatterers of different kinds, is subdivided into N thin elementary sublayers (Fig. 3). For each sublayer, both the upper and lower half-spaces are subdivided into N_θ discrete intervals of incidence and scattering off-normal angles of θ and θ_s , respectively; the interval amplitude is $\Delta\theta$. The matrix elements of $[\sigma]$ are averaged over θ and θ_s angles belonging to the j th and i th intervals, respectively. In this way the $\sigma_{ijpq}^- (\varphi_s - \varphi)$ and $\sigma_{ijpq}^+ (\varphi_s - \varphi)$ functions are obtained, representing average polarized bistatic scattering cross sections in the upper and lower half-spaces, respectively. Similarly, the matrix elements of $[\sigma_e]$ are averaged over θ angles belonging to the j th interval, obtaining the σ_{ejpq} elements.

The sublayer scattering is described by the upper half-space scatter matrices S^- and the lower half-space scatter matrices S^+ . Each element of an S^- matrix represents the ratio I_{sip} / I_{jq} between p -polarized ($p = 1, \dots, 4$) specific intensity ($\text{W}/\text{m}^2 \text{st}$) scattered into the i th angular interval of the upper half-space and the q -polarized ($q = 1, \dots, 4$) specific intensity incident from the j th angular interval of the upper half-space. Similarly, the S^+ matrix elements represent the I_{tip} / I_{jq} ratios, where I_{tip} is the specific intensity scattered towards the lower half-space. The dependence on $\varphi_s - \varphi$ is expressed in Fourier series, so that the number N_θ of S^- and S^+ matrices is equal to the number of series terms. For the m th Fourier term, it is shown by Ferrazzoli and Guerriero (1995) that the elements of S^- and S^+ matrices are given by

$$S_{ijpqm}^- = \frac{n\Delta z \Delta \theta \sin \theta_j}{4\pi \cos \theta_{si}} a_m \mathcal{F}_m \{ \sigma_{ijpq}^- (\varphi_s - \varphi) \}, \quad (3)$$

$$S_{ijpqm}^+ = \frac{n\Delta z \Delta \theta \sin \theta_j}{4\pi (-\cos \theta_{si})} a_m \mathcal{F}_m \{ \sigma_{ijpq}^+ (\varphi_s - \varphi) \}. \quad (4)$$

Δz (m) is the sublayer thickness, while n (m^{-3}) is the scatterer density. The $\mathcal{F}_m \{ \}$ symbol indicates the m th Fourier term. The a_m parameter is given by

$$a_m = \begin{cases} 2\pi & \text{if } m = 0, \\ \pi & \text{if } m > 0. \end{cases}$$

For each Fourier term m , the $4N_\theta \times 4N_\theta$ S_m^- and S_m^+ matrices are obtained, given by

$$S_m^- = \begin{bmatrix} S_{11m}^- & S_{12m}^- & S_{13m}^- & S_{14m}^- \\ S_{21m}^- & S_{22m}^- & S_{23m}^- & S_{24m}^- \\ S_{31m}^- & S_{32m}^- & S_{33m}^- & S_{34m}^- \\ S_{41m}^- & S_{42m}^- & S_{43m}^- & S_{44m}^- \end{bmatrix}, \quad (5)$$

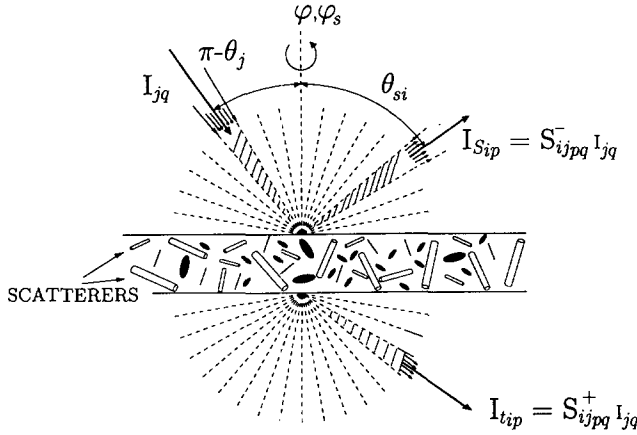


Figure 3. Representation of a scatterer sublayer: θ_j , θ_{si} = discretized off-normal angles of incidence and scattering directions, φ , φ_s = azimuth angles of incidence and scattering directions, I_{jq} = q -polarized incident specific intensity, I_{sip} = p -polarized upward scattered specific intensity, and I_{tip} = p -polarized downward scattered specific intensity.

$$S_m^+ = \begin{bmatrix} S_{11m}^+ & S_{12m}^+ & S_{13m}^+ & S_{14m}^+ \\ S_{21m}^+ & S_{22m}^+ & S_{23m}^+ & S_{24m}^+ \\ S_{31m}^+ & S_{32m}^+ & S_{33m}^+ & S_{34m}^+ \\ S_{41m}^+ & S_{42m}^+ & S_{43m}^+ & S_{44m}^+ \end{bmatrix}. \quad (6)$$

S_{pqm}^- and S_{pqm}^+ ($p, q = 1, \dots, 4$) are $N_\theta \times N_\theta$ square matrices; their elements correspond to the N_θ angular intervals defined in Figure 3.

In order to correctly include both the scattering effects and the forward propagation effects, the downward scattered specific intensity, expressed by the S_m^+ matrices, must be added to the forward propagating specific intensity, which is affected by attenuation and phase delay. To do this, a $4N_\theta \times 4N_\theta$ forward propagation T^+ matrix is computed, given by (Ferrazzoli and Guerriero, 1995)

$$T^+ = \mathbf{1} - \begin{bmatrix} k_{e11} & 0 & 0 & 0 \\ 0 & k_{e22} & 0 & 0 \\ 0 & 0 & k_{e33} & k_{e34} \\ 0 & 0 & k_{e43} & k_{e44} \end{bmatrix}. \quad (7)$$

k_{epq} are $N_\theta \times N_\theta$ matrices with the main diagonal elements given by (Ferrazzoli and Guerriero, 1995)

$$k_{eijpq} = \frac{n\Delta z}{\cos \theta_j} \cdot \sigma_{epq} \quad (8)$$

while off-diagonal elements are 0; $\mathbf{1}$ is a $4N_\theta \times 4N_\theta$ unit matrix. The total downward transmitted polarized specific intensity is expressed by transmission matrices T_m given by

$$T_m = S_m^+ + T^+. \quad (9)$$

The various contributions are then combined as follows: If two adjacent elementary sublayers are characterized by scattering and transmission matrices S_{1m}^-, T_{1m} and S_{2m}^-, T_{2m} , respectively, the corresponding matrices of the layer composed by the two sublayers are obtained through the matrix “doubling” algorithm (Fung, 1994) that is,

$$S_m^- = S_{1m}^- + T_{1m} S_{2m}^- (1 - S_{1m}^- S_{2m}^-)^{-1} T_{1m}, \quad (10)$$

and, analogously,

$$T_m = T_{2m} (1 - S_{1m}^- S_{2m}^-)^{-1} T_{1m}. \quad (11)$$

By reiterating this procedure, the N sublayers are successively combined, and the Fourier components of the scattering and transmission matrices S_{vm}^- and T_{vm} of the whole canopy are computed.

The number N of elementary layers into which the canopy is subdivided may be selected as the minimum value beyond which the finally computed backscatter coefficient does not vary by more than a given limit (e.g., 0.5 dB).

Soil

A soil element of area ΔA may be described by a 4×4 modified Mueller matrix $[\sigma_g]$ similar to that given in (1) for a single scatterer. Azimuthal symmetry is assumed also in this case; therefore, the elements of $[\sigma_g]$ are functions of θ , θ_s , and $\varphi_s - \varphi$.

The models of scattering from rough soil surfaces require as input data the permittivity, the standard deviation of surface height h_g and the correlation length l_g . A Gaussian correlation function is assumed. The small perturbation model is used for low h_g/λ values (λ is the wavelength) while the geometrical optics model is used for high h_g/λ values (Kuga et al., 1990). The permittivity is related to the moisture by the semiempirical formula proposed by Ulaby et al. (1986a).

The 16 matrix elements computed by the surface model (using formulas 4.45 or 4.130 given by Kuga et al., 1990) are normalized with respect to ΔA and will be indicated as σ_{gijpq}^o (θ , θ_s , $\varphi_s - \varphi$) (“polarized bistatic scattering coefficients”). Assuming the subdivision in angular intervals described in Figure 3, a σ_{gijpq}^o ($\varphi_s - \varphi$) function may be obtained, which gives the p -polarized specific intensity in the i th angular interval for a q -polarized specific intensity incident from the j th angular interval. Only scattering in the upper half-space has to be considered for the soil.

Similarly to the case of a vegetation layer, the dependence on $\varphi_s - \varphi$ is expressed in Fourier series and N_φ matrices S_{gm}^- are obtained. For a Fourier term m , the element of a S_{gm}^- matrix is given by (Ferrazzoli and Guerriero, 1995)

$$S_{gijpqm}^- = \frac{\Delta \theta \sin \theta_j}{4\pi \cos \theta_{si}} \cdot a_m \mathfrak{F}_m \{ \sigma_{gijpq}^o(\varphi_s - \varphi) \}. \quad (12)$$

Large Vertical Elements

Many crops are characterized by the presence of vertical stalks located between the soil and the scatterer layer. The bistatic scattering patterns of these elements are much peaked in the conical surface containing the forward direction. Therefore, only two effects are considered: extinction and soil-stalk double-bounce specular reflection ("corner reflector"). Scattering effects in other directions are neglected.

Propagation is described, for a given incidence angular interval, by a 4×4 extinction matrix \mathbf{T}_{sij} . According to the theory developed in Tsang et al. (1985) and Lopez et al. (1991),

$$\mathbf{T}_{sij} = \begin{bmatrix} \langle \exp(-\tau_1) \rangle & 0 & 0 & 0 \\ 0 & \langle \exp(-\tau_2) \rangle & 0 & 0 \\ 0 & 0 & \langle \exp(-\tau) \cos \delta \rangle & \langle -\exp(-\tau) \sin \delta \rangle \\ 0 & 0 & \langle \exp(-\tau) \sin \delta \rangle & \langle \exp(-\tau) \cos \delta \rangle \end{bmatrix}, \quad (13)$$

where

$$\begin{aligned} \tau_1 &= \frac{4\pi N_s}{k \cos \theta} \text{Im}(f_{svv}^r), \\ \tau_2 &= \frac{4\pi N_s}{k \cos \theta} \text{Im}(f_{shh}^r), \\ \tau &= \frac{2\pi N_s}{k \cos \theta} [\text{Im}(f_{svv}^r) + \text{Im}(f_{shh}^r)], \\ \delta &= \frac{2\pi N_s}{k \cos \theta} [\text{Re}(f_{svv}^r) - \text{Re}(f_{shh}^r)]. \end{aligned}$$

N_s is the stalk density (m^{-2}). f_{svv}^r and f_{shh}^r are the stalk forward scattering amplitudes at VV and HH polarizations, respectively. Averaging is carried out within the j th angular interval.

The backscatter coefficient due to the soil-stalk specular reflection ("corner reflector") may be expressed, for the j th angular interval, by a 4×4 matrix given by

$$[\sigma_{sg}^o]_{ij} = \mathbf{T}_{sij} \{ [\sigma_s]_{ij} \mathbf{\Gamma}_j + \mathbf{\Gamma}_j [\sigma_s]_{ij} \} \mathbf{T}_{sij} \quad (14)$$

$[\sigma_s]_{ij}$ is the stalk 4×4 modified Mueller matrix in the specular direction for the j th angular interval of incidence.

$$[\sigma_s]_{ij} = 4\pi N_s$$

$$\times \begin{bmatrix} \langle |f_{svv}^r|^2 \rangle \langle |f_{svh}^r|^2 \rangle & 0 & 0 \\ \langle |f_{shv}^r|^2 \rangle \langle |f_{shh}^r|^2 \rangle & 0 & 0 \\ 0 & 0 & \langle \text{Re}(f_{svv}^r f_{shh}^r) \rangle \langle -\text{Im}(f_{svv}^r f_{shh}^r) \rangle \\ 0 & 0 & \langle \text{Im}(f_{svv}^r f_{shh}^r) \rangle \langle \text{Re}(f_{svv}^r f_{shh}^r) \rangle \end{bmatrix}, \quad (15)$$

where f_{sq}^r is the single stalk scattering amplitude in the specular direction at q polarization; $f_{spq}^r = 0$ if $p \neq q$, due to the vertical orientation. Averaging is carried out within the j th angular interval.

$\mathbf{\Gamma}_j$ is the soil specular reflection 4×4 modified Mueller matrix, given by

$$\mathbf{\Gamma}_j = \exp[-(4\pi h_g \cos \theta_j / \lambda)^2]$$

$$\times \begin{bmatrix} \langle |R_v|^2 \rangle & 0 & 0 & 0 \\ 0 & \langle |R_h|^2 \rangle & 0 & 0 \\ 0 & 0 & \langle \text{Re}(R_v R_h^*) \rangle & \langle -\text{Im}(R_v R_h^*) \rangle \\ 0 & 0 & \langle \text{Im}(R_v R_h^*) \rangle & \langle \text{Re}(R_v R_h^*) \rangle \end{bmatrix}. \quad (16)$$

Averaging is carried out within the j th angular interval. R_q is the Fresnel smooth-surface reflection coefficient at q polarization, and h_g is the soil roughness standard deviation.

Final Computation

Canopy and soil contributions are combined through the following matrix operation:

$$\mathbf{S}_{vgn}^- = \mathbf{S}_{vm}^- + \mathbf{T}_{vm} \mathbf{S}_{sgm}^- (\mathbf{I} - \mathbf{S}_{vm}^- \mathbf{S}_{sgm}^-)^{-1} \mathbf{T}_{vm}, \quad (17)$$

where

$$\mathbf{S}_{sgm}^- = \mathbf{T}_s \mathbf{S}_{gm}^- \mathbf{T}_s. \quad (18)$$

\mathbf{T}_s is a $4N_\theta \times 4N_\theta$ matrix whose structure is similar to that of \mathbf{S}_m^- and \mathbf{S}_m^+ matrices [(5) and (6)]; in this case, all elements with $i \neq j$ are null, while \mathbf{T}_{sij} are those reported in (13). In this way the $N_\theta/2 + 1$ Fourier scattering matrices of canopy and soil scattering are obtained.

The backscatter in the j th angular interval may be expressed by a 4×4 matrix $[\sigma^o]_{ij}$ whose elements are given by (Ferrazzoli and Guerriero, 1995)

$$\sigma_{ijpq}^o = \frac{4\pi}{\Delta\theta} (\cot \theta_j) S'_{vgijpq}(\pi) + T_{vijqq} \sigma_{sgijpq}^o T_{vijpp}. \quad (19)$$

T_{vijqq} and T_{vijpp} are the scatterer layer transmissivities for q and p polarization, respectively, and

$$S'_{vgijpq}(\pi) = \sum_{m=0}^{N_\theta/2+1} \frac{1}{a_m} \mathbf{S}_{vgijpqm}^- \cos(m\pi). \quad (20)$$

We recall that p and q are the indexes of modified Stokes parameters associated with backscattering and incidence polarization, respectively. Consider an elliptically polarized electromagnetic field, characterized by an orientation angle ψ and an ellipticity angle χ incident from the j th angular interval on the canopy. To compute the backscatter coefficient $\sigma_{ij}^o(\psi_s, \chi_s, \psi, \chi)$ associated with a scattered field with orientation angle ψ_s and ellipticity angle χ_s , the "polarization synthesis" has to be carried out. According to the theory presented by Van Zyl and Ulaby (1990), the following relation holds:

$$\sigma_{ij}^o(\psi_s, \chi_s, \psi, \chi) = \mathbf{Y}_s^T ([\mathbf{v}][\mathbf{v}]^T)^{-1} [\sigma^o]_{ij} \mathbf{Y}, \quad (21)$$

where the T suffix indicates transpose and

$$[\mathbf{v}] = \begin{bmatrix} 1 & 0 & 0 & 0 \\ 0 & 1 & 0 & 0 \\ 0 & 0 & 1 & 1 \\ 0 & 0 & -j & j \end{bmatrix}, \quad (22)$$

$$\mathbf{Y} = \begin{bmatrix} 0.5(1 + \cos 2\psi \cos 2\chi) \\ 0.5(1 - \cos 2\psi \cos 2\chi) \\ \sin 2\psi \cos 2\chi \\ \sin 2\chi \end{bmatrix}, \quad (23)$$

$$\mathbf{Y}_s = \begin{bmatrix} 0.5(1 + \cos 2\psi_s \cos 2\chi_s) \\ 0.5(1 - \cos 2\psi_s \cos 2\chi_s) \\ \sin(2\psi_s) \cos(2\chi_s) \\ \sin(2\chi_s) \end{bmatrix}. \quad (24)$$

Finally, it is noted that the $[\sigma^\circ]_{ij}$ elements have the same polarimetric significance as those of $[\sigma]$ given in (1), although the latter was bistatic and was computed for a single scatterer; as a consequence, it can be shown with simple algebraic manipulations that the phase difference between VV and HH channels is given by

$$\Delta\phi_{ij} = \arctan \frac{\sigma_{ij43}^\circ - \sigma_{ij34}^\circ}{\sigma_{ij33}^\circ + \sigma_{ij44}^\circ}. \quad (25)$$

COMPARISON WITH EXPERIMENTAL RESULTS

The Experiment

In the summer of 1991, in the framework of the Multisensor Airborne Campaign (MAC Europe 91), some European sites were overflown by the NASA-JPL AIRSAR (Held et al., 1988), on board a DC-8 aircraft. The system operates at P (0.45 GHz), L (1.2 GHz), and C (5.3 GHz) bands, with a pixel size of 6.6 m in range and 12 m in azimuth. In particular, the Italian Montespertoli site, located near Florence, was imaged at three different incidence angles (20°, 35° and 50°) and on three dates (22, 29 June and 14 July). Calibration was carried out by means of three corner reflectors, using the procedure suggested by Van Zyl (1990). The absolute accuracy of σ° values is estimated to be ± 1 dB. Details about flights and calibration are given by Baronti et al. (1995) and Ferrazzoli et al. (1995b). Within the site, an agricultural area, located close to the Pesa river, was selected and ground data were measured over some fields. Measurements were made of the main soil and vegetation parameters, like soil moisture (%), soil roughness (cm), plant moisture (%), total plant water content (kg/m^2), and leaf area index (m^2/m^2). Ground data were averaged over four sampling points per field and over three plants per sampling point. The maximum PWC standard error was $\sim 0.5 \text{ kg}/\text{m}^2$.

Since crop growth monitoring is an important remote sensing application, in this section we test the ability of the model in reproducing the radar sensitivity to plant water content (PWC), which is a significant crop growth indicator. To this aim, we compare theoretical and experimental polarimetric features of three farm-

ers sunflower fields, since they showed a wide variety of PWC values during the three flights. Two fields, which had been sowed at the end of April, were green and healthy during the whole campaign period. Their average heights were ~ 95 cm during the first flight, ~ 110 cm during the second flight, and ~ 160 cm during the third flight, when they were flowering. The third field was sowed at the end of May. Its average heights during the three flights were ~ 40 cm, ~ 65 cm, and ~ 110 cm, respectively. It was green during the first two flights, while it suffered some stress during the last flight, when the “eye” was appearing.

We consider L band data, which are fairly well correlated with sunflower PWC (Ferrazzoli et al., 1995b) and the higher incidence angles (35° and 50°) for which absolute calibration is more reliable (Baronti et al., 1995).

Model Inputs

To simulate sunflower scattering, the scheme indicated in Figure 1 has been applied. The Rayleigh–Gans approximation has been used to compute scattering and extinction properties of discs and small cylinders (stems), while the “infinite length” cylinder approximation has been applied for vertical stalks; the soil scattering has been computed by the small perturbation model, for which the conditions of validity indicated by Kuga et al. (1990) were satisfied at L band.

Some parameters, to be given as inputs to the model, have been related to PWC by empirical relationships, derived on average by measured ground data:

- LAI (leaf area index) = $0.9 \times \text{PWC}$.
- Vertical cylinder (stalk) height (cm):

$$h_s = \begin{cases} 0.75(60 - 10 \times \text{LAI}) \times \text{LAI} & (\text{LAI} < 3) \\ 0.75 \times 30 \times \text{LAI} & (\text{LAI} > 3). \end{cases}$$

- Vertical cylinder (stalk) diameter (cm):
 $d_s = 1.5 + 0.25 \times \text{LAI}$.

Some parameters have been assumed to be constant, since they showed relatively small variations among the various fields and during the campaign period:

- Soil roughness standard deviation: $h_g = 1.25$ cm.
- Soil roughness average slope: $m_g = 0.3$.
- Stalk density: $N_s = 7.9 \text{ m}^{-2}$.
- Disc (leaf) thickness: $\delta_d = 0.025$ cm.
- Disc (leaf) diameter: $d_d = 16$ cm.
- Disc (leaf) orientation distribution:

$$\begin{aligned} -0 < \alpha_d < 2\pi, & \quad p(\alpha_d) = 1 \\ -0 < \beta_d < \pi/2, & \quad p(\beta_d) = 1, \\ -\gamma_d & = 0 \end{aligned}$$

- Inclined cylinder (stem) diameter: $d_c = 0.5$ cm.
- Inclined cylinder (stem) length: $l_c = 40 \times d_c$.
- Inclined cylinder (stem) orientation distribution:
 - $-0 < \alpha_c < 2\pi$, $p(\alpha_c) = 1$,
 - $-45^\circ < \beta_c < 85^\circ$, $p(\beta_c) = 1$,
 - $-\gamma_c = 0$.
- Dry matter density: $d_d = 0.25$ g/cm³.

The moistures of soil and plant elements were slightly decreasing during the campaign period. On 26 June the following values were measured on average (also the corresponding permittivities are given):

- Volumetric soil moisture: 17.5% ($\epsilon_g = 9.4 - j0.6$).
- Vertical stalk moisture (by weight): 90% ($\epsilon_s = 57.0 - j14.2$).
- Stem and leaf moisture (by weight): 85% ($\epsilon_v = 43.8 - j10.4$).

On 14 July measurements results were the following:

- Volumetric soil moisture: 10% ($\epsilon_g = 5.9 - j0.4$).
- Vertical stalk moisture (by weight): 85% ($\epsilon_s = 43.8 - j10.4$).
- Stem and leaf moisture (by weight): 80% ($\epsilon_v = 34.7 - j7.9$).

Computations have been carried out for both the above indicated moisture conditions. Intermediate values were measured during the second flight (29 June).

Most of the above-mentioned model inputs have directly been derived by ground measurements. For orientation distributions and inclined cylinder dimensions reasonable assumptions, based on crop visual inspections, have been done. Disc diameters have been chosen to be equal to leaf diameters since, in the particular case of sunflower at L band, leaves are almost circular and flat with respect to the wavelength.

The scheme of Figure 1 does not include some complex elements, like flowers, which appeared in two fields during the last flight; moreover, it assumes an azimuthal symmetry condition which was roughly satisfied in the real fields. In spite of these approximations, some important features of experimental data are well represented by the model, as will be indicated below.

Results

Model predicted and experimental backscatter coefficients of sunflower fields as a function of PWC are shown in Figure 4 for HH (a), HV (b), and VV (c) polarization and in Figure 5 for RR (a), RL (b), 45-45 (c), and 45-135 (d) polarization. RR and RL symbols indicate circular copolar and circular crosspolar polarizations, respectively. For RR, $Y = [0.5, 0.5, 0, -1]$ and $Y_s = [0.5, 0.5, 0, -1]$ while, for RL, $Y = [0.5, 0.5, 0, 1]$ and

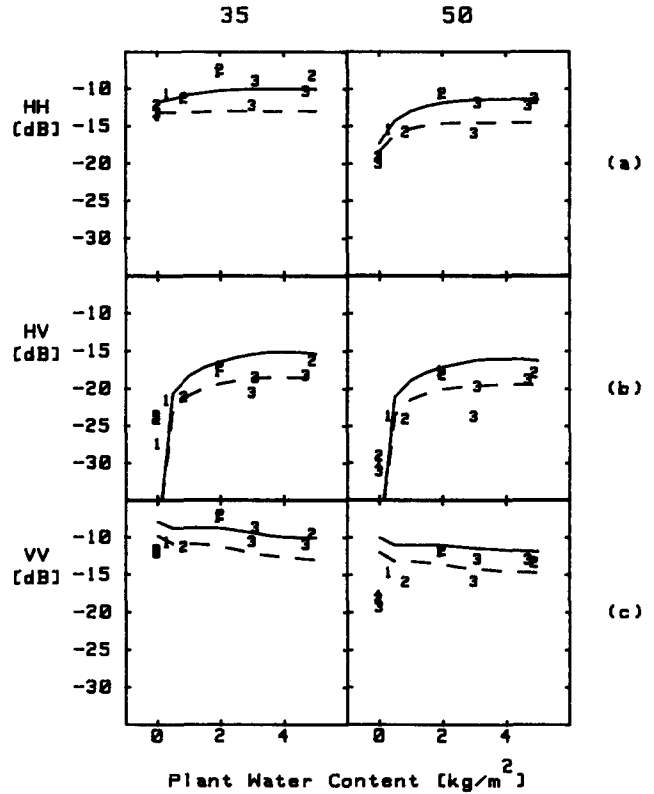


Figure 4. Backscatter coefficient σ^o (dB) vs PWC (kg/m²) at L band. $\theta = 35^\circ$ (left side), 50° (right side). Polarizations: a) HH; b) HV; c) VV. Labels correspond to experimental data and indicate flight date [1] 22 June 1991; 2) 29 June 1991; 3) 14 July 1991]. Lines show model predictions for flight 1 (continuous) and 3 (dashed).

$Y_s = [0.5, 0.5, 0, -1]$. 45-45 and 45-135 symbols indicate copolar and crosspolar polarizations (respectively) when the incoming field is at 45° with respect to the incidence plane; for 45-45, $Y = [0.5, 0.5, 1, 0]$ and $Y_s = [0.5, 0.5, 1, 0]$ while, for 45-135, $Y = [0.5, 0.5, -1, 0]$ and $Y_s = [0.5, 0.5, 1, 0]$. Figure 6 shows the VV-HH phase difference vs. the PWC. In the three figures, continuous lines indicate predicted values for the first flight, dashed lines indicate predicted values for the third flight, and labels correspond to experimental data and indicate the flight number. Three sunflower fields were observed during the flights. Also data measured over a bare soil, whose roughness was close to that of sunflower fields, have been included for comparison; in the figures, they correspond to samples with PWC = 0.

Observation of theoretical curves suggests the following considerations:

- Trends are flat at VV, RL, and 45-45 polarization, while an appreciable sensitivity to PWC is observed at HV, RR, and 45-135 polarization, with saturation occurring at ~ 2 kg/m². At HH polarization the trend is flat at 35° but becomes increasing at 50° .

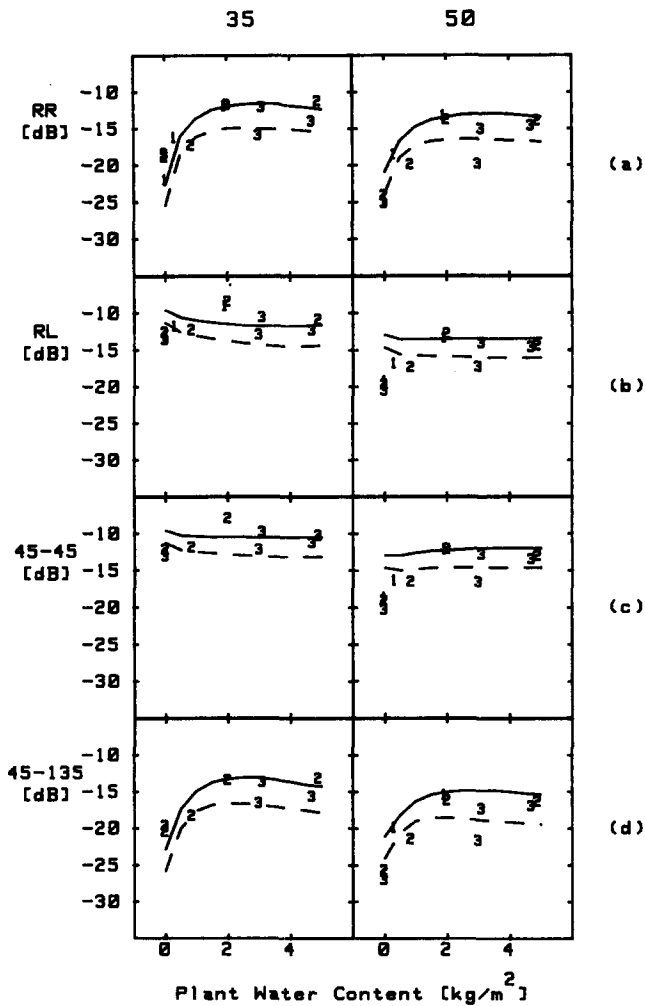


Figure 5. Backscatter coefficient σ^0 (dB) vs. PWC (kg/m^2) at L band. $\theta = 35^\circ$ (left side), 50° (right side). Polarizations: a) RR; b) RL; c) 45-45; d) 45-135. Labels correspond to experimental data and indicate flight date [1] 22 June 1991; [2] 29 June 1991; [3] 14 July 1991]. Lines show model predictions for flight 1 (continuous) and 3 (dashed).

- VV-HH phase is negative, showing a minimum at intermediate PWC values. This minimum is due to the soil-stalk double bounce effect, since the latter, which has an important influence on the phase, is absent at low PWCs while is quenched by stem and leaf attenuation at high PWC.
- Moisture effects are important. Differences between continuous and dashed lines, which correspond to moisture conditions of 26 June and 14 July (respectively) are up to ~ 4 dB at 45-135 polarization, up to ~ 3 dB at the other polarizations; in the phase, differences up to $\sim 30^\circ$ are noted (see Fig. 6).

When model results are compared with experimental data, the following considerations apply.

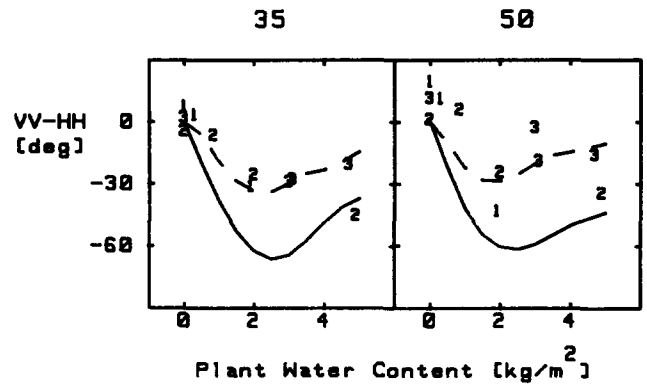


Figure 6. VV-HH phase difference (deg) vs. PWC (kg/m^2) at L band. $\theta = 35^\circ$ (left side), 50° (right side). Labels correspond to experimental data and indicate flight date [1] 22 June 1991, [2] 29 June 1991, [3] 14 July 1991]. Lines show model predictions for flight 1 (continuous) and 3 (dashed).

- In Figures 4 and 5 the maximum differences between experimental and theoretical data are observed at low PWCs, 50° , VV and (to a lesser extent) RL and 45-45 polarization. The problem is due to the surface small perturbation model, which overestimates the VV-polarized backscatter coefficient, as noted also in other experiments by Ferrazzoli and Guerriero (1994) and Oh et al. (1992). This discrepancy may slightly be mitigated, but not eliminated, by using the integral equation model (Coppo et al., 1994). In all the other plots of Figures 4 and 5, the PWC trends are well reproduced by the model, and most of the samples corresponding to the third flight show a lower backscatter, as the theoretical curves indicate. Discrepancies are noted in a limited number of samples and generally do not exceed 2 dB.
- The model tends to overestimate the negative VV-HH phase difference. Probably some assumptions, like vertical stalks, azimuthal symmetry, etc., which are not completely satisfied in a real environment, influence the phase to a greater extent than the amplitude. However, the phase trend vs. PWC is fairly well reproduced.

CONCLUSION AND DISCUSSION

A model has been described which simulates the polarimetric features of agricultural fields. Model simulations have been compared with experimental results obtained at L-band by the NASA-JPL AIRSAR over sunflower fields in Italy. Predicted and experimental results agree in indicating HV, RR, and 45-135 polarizations to show the best sensitivities to crop growth. A general agreement between theory and experiments is also observed when

moisture effects are investigated. However, a discrepancy is noted over bare soils, particularly at VV polarization, due to inaccuracies of available surface models.

The VV–HH phase difference shows a non-monotonic trend as a function of plant water content; for vegetated fields the phase differences are negative and the model tends to slightly overestimate them.

Results of this article indicate that an L-band radar is helpful to estimate the biomass of crops with wide leaves, like sunflower, during the growing season. σ° saturation occurs at $\sim 2 \text{ kg/m}^2$, but a greater amount of experimental data are needed, covering also the drying season, to deeply understand the role of both wet and dry biomass, and refine the assumptions used in the previous section to give inputs to the model. Experimental results presented by Bouman and Hoekman (1993), Ferrazzoli et al. (1992), and Ulaby et al. (1986b) indicate that also copolar radars are sensitive to crop biomass. However, both experimental and theoretical results of this article show that, in the growing period, the influence of biomass on σ° is much higher at HV polarization than at HH and VV polarization. Finally, the performance of a fully polarimetric radar does not appear to be significantly better than that of a radar measuring only σ_{HH}° , σ_{VV}° , and σ_{HV}° to monitor growth of a single agricultural species. Polarimetry shows a higher potential in discriminating among different vegetation species, as the results given by de Matthaeis et al. (1994) and Baronti et al. (1995) indicate.

This work has been partially supported by ASI, Agenzia Spaziale Italiana.

REFERENCES

- Attema, E. P. W., and Ulaby, F. T. (1978), Vegetation modeled as a water cloud, *Radio Sci.* 13:357–364.
- Baronti, S., Del Frate, F., Ferrazzoli, P., Paloscia, S., Pampaloni, P., and Schiavon, G. (1995), SAR polarimetric features of agricultural areas, *Int. J. Remote Sens.*, forthcoming.
- Bouman, B. A. M., and Hoekman, D. H. (1993), Multi-temporal, multi-frequency radar measurements of agricultural crops during the Agriscatt-88 campaign in The Netherlands, *Int. J. Remote Sens.* 14:1595–1614.
- Chauhan, N. S., Le Vine, D. M., and Lang, R. H. (1994), Discrete scatter model for microwave radar and radiometer response to corn: comparison of theory and data, *IEEE Trans. Geosci. Remote Sens.* 32:416–426.
- Churchill, P. N., and Attema, E. P. W. (1992), The MAESTRO-1 European Airborne Polarimetric Synthetic Aperture Radar Campaign, in *MAESTRO-1/AGRISCATT. Radar Techniques for Forestry and Agricultural Applications, Proceedings of the ESA Workshop*, ESTEC, Noordwijk, The Netherlands, 6–7 March, European Space Agency WPP-31, Paris, pp. 209–216.
- Coppo, P., Luzi, G., Del Frate, F., and Schiavon, G. (1994), Microwave surface scattering from rough soils: a comparison between models and experimental data collected with airborne radars, in *Proceedings, Progress in Electromagnetic Research Symposium*, ESA WPP-073, Noordwijk, The Netherlands, July.
- de Matthaeis, P., Schiavon, G., and Solimini, D. (1994), Effect of scattering mechanisms on polarimetric features of crops and trees, *Int. J. Remote Sens.* 15:2917–2930.
- El-Rayes, M. A., and Ulaby, F. T. (1987), Microwave dielectric spectrum of vegetation – Part I: Experimental observations, *IEEE Trans. Geosci. Remote Sens.* 25:541–549.
- Eom, H. J., and Fung, A. K. (1984), A scatter model for vegetation up to Ku-band, *Remote Sens. Environ.* 15:185–200.
- Eom, H. J., and Fung, A. K. (1986), Scattering from a random layer embedded with dielectric needles, *Remote Sens. Environ.* 19:139–149.
- Ferrazzoli, P., and Guerriero, L. (1994), Interpretation and model analysis of MAESTRO-1 Flevoland data, *Int. J. Remote Sens.* 15:2901–2915.
- Ferrazzoli, P., and Guerriero, L. (1995), Radar sensitivity to tree geometry and woody volume: a model analysis, *IEEE Trans. Geosci. Remote Sens.* 33:360–371.
- Ferrazzoli, P., Guerriero, L., and Solimini, D. (1991), Numerical model of microwave backscattering and emission from terrain covered with vegetation, *Appl. Comput. Electromagn. Soc. J.* 6:175–191.
- Ferrazzoli, P., Paloscia, S., Pampaloni, P., Schiavon, G., Solimini, D., and Coppo, P. (1992), Sensitivity of microwave measurements to vegetation biomass and soil moisture content: a case study, *IEEE Trans. Geosci. Remote Sens.* 30:750–756.
- Ferrazzoli, P., Guerriero, L., Paloscia, S., and Pampaloni, P. (1995a), Modeling X and Ka band emission from leafy vegetation, *J. Electromagn. Waves Appl.* 9:393–406.
- Ferrazzoli, P., Luciani, S., Schiavon, G., et al. (1995b), Dependence of polarimetric SAR data on vegetation properties: results for the Montespertoli Italian site, in *Proceedings of MAC Europe '91 Final Results Workshop*, Lenggries, Germany, 4–6 October, European Space Agency WPP-88, Paris, pp. 71–81.
- Fung, A. K. (1994), *Microwave Scattering and Emission Models and Their Applications*, Artech House, Norwood, MA, pp. 339–372.
- Held, D. N., Brown, W. E., Freeman, A., et al. (1988), The NASA/JPL Multifrequency, multipolarization airborne SAR system, in *Proceedings of 1988 International Geoscience and Remote Sensing Symposium*, Edinburgh, 12–16 September, IEEE 88CH2497-6, pp. 345–348.
- Ishimaru, A. (1978) *Wave Propagation and Scattering in Random Media*, Academic, London, pp. 1–40.
- Karam, M. A., and Fung, A. K. (1988), Electromagnetic scattering from a layer of finite length, randomly oriented, dielectric, circular cylinders over a rough interface with application to vegetation, *Int. J. Remote Sens.* 9:1109–1134.
- Kuga, J., Whitt, M. W., McDonald, K. C., and Ulaby, F. T. (1990), *Radar Polarimetry for Geoscience Applications* (F. T. Ulaby and C. Elachi, Eds.), Artech House, Norwood, MA, Chap. 4.
- Le Vine, D. M., Meneghini, R., Lang, R. H., and Seker, S. S. (1983), Scattering from arbitrarily oriented dielectric disks

- in the physical optics regime, *J. Opt. Soc. Am.* 73:1255–1262.
- Lopez, A., Mougin, E., Le Toan, T., Karam, M. A., and Fung, A. K. (1991), A simulation study on the influence of leaf orientation on elliptically polarized microwave propagation in a coniferous forest, *J. Electromagn. Waves Appl.* 5:753–776.
- Oh, Y., Sarabandi, K., and Ulaby, F. T. (1992), An empirical model and an inversion technique for radar scattering from bare soil surfaces, *IEEE Trans. Geosci. Remote Sens.* 30:370–381.
- Prevot, L., Dechambre, M., Taconet, O., Vidal-Majar, D., Normand, M., and Galle, S. (1993), Estimating the characteristics of vegetation canopies with airborne radar measurements, *Int. J. Remote Sens.* 14:2803–2818.
- Schiffer, R., and Thielheim, K. O. (1979), Light scattering by dielectric needles and disks, *J. Appl. Phys.* 50:2476–2483.
- Tourè, A., Thompson, K. P. B., Edwards, G., Brown, R. J., and Brisco, B. G. (1994), Adaptation of the MIMICS back-scattering model to the agricultural context—wheat and canola at L and C bands, *IEEE Trans. Geosci. Remote Sens.* 32:47–61.
- Tsang, L., Kong, J. A., and Shin, R. T. (1985), *Theory of Microwave Remote Sensing*, Wiley-Interscience, New York, pp. 119–168.
- Ulaby, F. T., and Dobson, M. C. (1989), *Handbook of Radar Statistics from Terrain*, Artech House, Norwood, MA.
- Ulaby, F. T., Moore, R. K., and Fung, A. K. (1986a), *Microwave Remote Sensing: Active and Passive, Vol. III—From Theory to Applications*, Artech House, Dedham, MA, pp. 2086–2104.
- Ulaby, F. T., Moore, R. K., and Fung, A. K. (1986b), *Microwave Remote Sensing: Active and Passive, Vol. III—From Theory to Applications*, Artech House, Dedham, MA, pp. 1848–1881.
- Ulaby, F. T., Held, D., Dobson, M. C., McDonald, K. C., and Senior, T. B. A. (1987), Relating polarization phase difference of SAR signals to scene properties, *IEEE Trans. Geosci. Remote Sens.* 25:83–92.
- Van Zyl, J. J. (1990), Calibration of polarimetric radar images using only image parameters and trihedral corner reflectors, *IEEE Trans. Geosci. Remote Sens.* 28:337–348.
- Van Zyl, J. J., and Ulaby, F. T. (1990), *Radar Polarimetry for Geoscience Applications* (F. T. Ulaby and C. Elachi, Eds.), Artech House, Norwood, MA, Chap. 2.
- Wickland, D. E., Murphy, R. E., and Janetos, A. C. (1993), Overview of MAC Europe '91 Campaign and NASA Airborne Imaging Spectrometry and Radar Programs, in *Proceedings of 25th ERIM International Symposium on Remote Sensing and Global Environmental Change*, Graz, Austria, 4–8 April, ERIM, Ann Arbor, MI, pp. I66–I73.
- Yueh, S. H., Kong, J. A., Jao, J. K., Shin, R. T., and Le Toan, T. (1992), Branching model for vegetation, *IEEE Trans. Geosci. Remote Sens.* 30:390–402.